Dominant Modes of Variability in the South Atlantic: A Study with a Hierarchy of Ocean–Atmosphere Models

REINDERT J. HAARSMA

Royal Netherlands Meteorological Institute, De Bilt, Netherlands

EDMO J. D. CAMPOS

Oceanographic Institute, University of Sao Paulo, Sao Paulo, Brazil

WILCO HAZELEGER AND CAMIEL SEVERIJNS

Royal Netherlands Meteorological Institute, De Bilt, Netherlands

ALBERTO R. PIOLA

Servico de Hidrografia Naval, Buenos Aires, Argentina

FRANCO MOLTENI

Abdus Salam International Centre for Theoretical Physics, Trieste, Italy

(Manuscript received 17 July 2003, in final form 13 September 2004)

ABSTRACT

Using an atmosphere model of intermediate complexity and a hierarchy of ocean models, the dominant modes of interannual and decadal variability in the South Atlantic Ocean are studied. The atmosphere Simplified Parameterizations Primitive Equation Dynamics (SPEEDY) model has T30L7 resolution. The physical package consists of a set of simplified physical parameterization schemes, based on the same principles adopted in the schemes of state-of-the-art AGCMs. It is at least an order of magnitude faster, whereas the quality of the simulated climate compares well with those models. The hierarchy of ocean models consists of simple mixed layer models with an increasing number of physical processes involved such as Ekman transport, wind-induced mixing, and wind-driven barotropic transport. Finally, the atmosphere model is coupled to a regional version of the Miami Isopycnal Coordinate Ocean Model (MICOM) covering the South Atlantic with a horizontal resolution of 1° and 16 vertical layers.

The coupled modes of mean sea level pressure and sea surface temperature simulated by SPEEDY–MICOM strongly resemble the modes as analyzed from the NCEP–NCAR reanalysis, indicating that this model configuration possesses the required physical mechanisms for generating these modes of variability. Using the ocean model hierarchy the authors were able to show that turbulent heat fluxes, Ekman transport, and wind-induced mixing contribute to the generation of the dominant modes of coupled SST variability. The different roles of these terms in generating these modes are analyzed. Variations in the wind-driven barotropic transport mainly seem to affect the SST variability in the Brazil–Malvinas confluence zone.

The spectra of the mixed layer models appeared to be too red in comparison with the fully coupled SPEEDY–MICOM model due to the too strong coupling between SST and surface air temperatures (SATs), resulting from the inability to advect and subduct SST anomalies by the mixed layer models. In SPEEDY–MICOM anomalies in the southeastern corner of the South Atlantic are subducted and advected toward the north Brazilian coast on a time scale of about 6 yr.

Corresponding author address: Dr. Reindert Haarsma, Royal Netherlands Meteorological Institute, Wilhelminalaan 10, 3730 AE De Bilt, Netherlands.
E-mail: haarsma@knmi.nl

1. Introduction

In recent years there has been an increasing effort to describe and understand decadal-to-interdecadal variability in the region of the tropical and South Atlantic.

Analyses of South Atlantic sea surface temperature (SST) and mean sea level pressure (MSLP) by Venegas et al. (1996, 1997, 1998) indicate the existence of interdecadal fluctuations in the coupled atmosphere–ocean system with a period of around 20 yr. It is suggested that the dominant physical processes involved in this interdecadal cycle include the horizontal advection of heat by the ocean currents and changes in the atmosphere–ocean heat fluxes through local air–sea interactions. Indications of variability on decadal-to-interdecadal time scales in SST are also found by Sterl (2001) and Moron et al. (1998). Analyzing the results of a multicentury integration of a coupled climate model, Wainer and Venegas (2002) detected multidecadal variability in the southern South Atlantic that they related to variability in the intensity of the Malvinas western boundary current.

Natural variability over the tropical Atlantic is dominated by two modes of variability: equatorial variability in the eastern cold tongue region and off-equatorial variability characterized by an anomalous cross-equatorial SST gradient (Ruiz-Barradas et al. 2000). The equatorial variability, also sometimes called the Atlantic ENSO analog, has mostly been explained by a "Bjerknes" feedback (Carton et al. 1996). In addition to this local Atlantic ENSO analog mode, Atlantic SST variability is also affected by the Pacific ENSO variability (Tourre et al. 1999). The cross-equatorial gradient in SST is often related to the wind–evaporation (WES) feedback involving an unstable thermodynamic ocean–atmosphere interaction between wind-induced heat fluxes and SST (Chang et al. 1997). However, the characterization of these modes as well as the existence of these feedbacks are still under debate (Xie 1999; Wang and Carton 2003).

Xie and Tanimoto (1998) suggested that the tropical and South Atlantic modes of decadal variability are part of a coherent pan-Atlantic decadal oscillation that also incorporates the decadal variability of the North Atlantic Oscillation (NAO). A connection between the North and South Atlantic was also suggested by Robertson et al. (2000), Watanabe and Kimoto (1999), and Okumura et al. (2001), who, in model studies, found the NAO to be sensitive to SST anomalies over the tropical and subtropical South Atlantic. Xie (1999) argues that the preferred time scales of the cross-equatorial SST gradient, if any, arise from forcing or interaction with the extratropics. An observed connection between midlatitude and tropical Atlantic variability was described by Rajagolapan et al. (1998). The existence of a connection between North and South Atlantic decadal variability is, however, still the subject of intense scientific debate (Hoerling et al. 2001).

El Niño is a strong controlling factor for climate fluctuations over the South American continent. However, during the last decades it has become clear that SST anomalies in the tropical and South Atlantic Ocean also have a significant effect. The influence of tropical Atlantic SST anomalies on the rainfall in Nordeste Brazil has been firmly established from observational studies (Hastenrath and Greischar 1993a,b; Carton et al. 1996) and explained by numerical modeling (Moura and Shukla 1981; Nobre and Shukla 1996; Gandu and Silva Dias 1998). In addition, Diaz et al. (1998) demonstrate that the rainfall in Uruguay and the Brazilian state of Rio Grande do Sul is linked with SST anomalies in the southwestern Atlantic Ocean. Analysis of river flows of southeastern South America by Robertson and Mechoso (1998) shows, apart from a strong ENSO signal, decadal variability associated with SST anomalies in the tropical North Atlantic and in the seas around Greenland, the latter suggesting a connection with the process of deepwater formation and the thermohaline circulation.

Cardoso (2001) recently found significant decadal variability in the temperature data in the metropolitan area of São Paulo, which is closely related to the SST in the South Atlantic Ocean. Gonçalves et al. (2001) also detected a significant impact of the South Atlantic SST anomalies on the development of cold surges in the tropical sector of South America. Positive SST anomalies off the southern coast of Brazil favor the development of intense cyclones associated with the cold air incursion in tropical South America. There are some indications of a long-term control on the frequency of these events, which may be associated with the decadal variability of the South Atlantic SST.

However, the relation between SST anomalies in the South Atlantic and the South American convergence zone (SACZ) is still somewhat enigmatic. Modeling studies with atmospheric general circulation models (AGCMs) (Robertson et al. 2003; Barreiro et al. 2002) indicate that South Atlantic SST anomalies do affect the strength and position of the SACZ. In particular, positive SST anomalies seem to enhance the intensity of SACZ. In contrast, an observational study by Robertson and Mechoso (2000) shows that enhanced intensity of SACZ is accompanied by negative SST anomalies underneath it. In a modeling study, Chaves and Nobre (2004) show that in case of a strong SACZ the enhanced cloudiness diminishes the incoming solar ra-

diation, thereby suggesting that the negative SST anomalies are the result and not the cause of the enhanced SACZ.

From this discussion it emerges that there are strong indications for the existence of decadal modes of variability in the climate system over the tropical and South Atlantic and that they have a significant impact on the climate over the South American continent. However, firmly based explanations of the dominant mechanisms are still lacking, although some suggestions have been made. This study aims to contribute toward the understanding of the dominant mechanisms of decadal variability in the tropical and South Atlantic.

In particular, we will focus on establishing the air–sea interaction processes in the South Atlantic area that are crucial for the explanation of observed patterns of climate variability on interannual to decadal time scales. One approach could be the analysis of the output of a state-of-the-art global coupled model. However, an important problem with the analysis of these models is that the conclusions mainly result from statistical inference. A real physical test would be to switch off the potential physical processes and analyze the results. Although in principle feasible in state-of-the-art atmosphere–ocean general circulation models (AOGCMs), it is in practice prohibitive owing to the complexity of the models and the large amount of required computer resources. Therefore, in addition to simulations with state-of-the-art climate models, studies with less complex climate models are needed for detailed investigation of the dominant processes on decadal time scales (Houghton et al. 2001). The results and hypotheses of these studies can than be confronted with results from state-of-the-art AOGCMs and observational datasets.

In this study, we have investigated the mechanisms for generating the dominant patterns of coupled decadal variability within the framework of a less complex model. An atmosphere model of intermediate complexity is coupled to an hierarchy of ocean models ranging from a simple passive mixed layer model to a state-of-the-art ocean model. This model setup allows us to perform sensitivity studies for investigating the dominant mechanisms.

Recently, Sterl and Hazeleger (2003, hereafter SH) have analyzed 52 yr of the National Centers for Environmental Prediction–National Center for Atmospheric Research (NCEP–NCAR) reanalysis data (Kalnay et al. 1996) and investigated the different contributions for the generation of the dominant patterns of coupled variability. They conclude that anomalous latent heat flux and wind-induced mixed layer deepening are the main processes leading to the observed SST variability, with a minor role for anomalous Ekman transport.

We have tested the conclusions of SH and investigated whether we could simulate the observed dominant patterns of coupled variability and evaluated the contributions of the different terms. Our approach can be considered as complementary to theirs. The main advantage is that each process can be studied in isolation and the effect of uncertain parameters can be evaluated.

Our results confirm basically those of SH, thereby firmly establishing their results. The main difference is the role of Ekman transport, which, according to our results, is also an important mechanism for generating coupled variability in the South Atlantic. In addition, we have also investigated the role of the wind-driven barotropic transport, which seems mainly to affect SST variability in the Brazil–Malvinas confluence zone.

2. Model structure

a. Atmosphere model

The atmosphere model used in this study is the Simplified Parameterizations Primitive Equation Dynamics (SPEEDY) model (Molteni 2003). It is an intermediate complexity model based on a spectral primitive equation core and a set of simplified parameterization schemes. The parameterization package has been especially designed to work in models with just a few vertical levels and is based on the same physical principles adopted in schemes of state-of-the-art AGCMs. The parameterized processes include large-scale condensation, convection, clouds, short- and longwave radiation, turbulent surface fluxes, and vertical diffusion. The horizontal resolution is T30 and the model has seven vertical levels. It is at least an order of magnitude faster than a state-of-the-art AGCM. The quality of the simulated climate compares well with that of more complex AGCMs. Some aspects of the systematic errors of SPEEDY are, in fact, typical of many AGCMs, although the error amplitude is higher than in those models.

b. Ocean models

The state-of-the-art ocean model used in this study is the Miami Isopycnal Coordinate Ocean Model (MICOM: Bleck et al. 1992). The model solves a momentum equation, a layer thickness equation, and tracer equations for temperature and salinity using an isopycnal vertical coordinate and a horizontal C grid on a Mercator projection. The isopycnal vertical coordinate implies that each layer has a homogeneous potential density. Only the upper layer has variable density on which the surface forcing acts. The model is fully

coupled with the atmosphere model and is forced by surface wind stress, turbulent heat fluxes, radiative fluxes, and a freshwater flux. No flux adjustment is used, and σ_0 is used as reference density. In the isopycnal layers below the upper-layer salinity is advected and the temperature is computed using the equation of state. In the upper layer the temperature is directly computed from the tracer equation. The basin is confined to the tropical and South Atlantic from 45°S to 20°N. The boundaries are closed and the isopycnal layers are relaxed toward a density and salinity profile obtained from Levitus and Boyer (1994) and Levitus et al. (1994). The same datasets are used for initialization of the temperature, salinity, and layer thickness distributions. The resolution is 1° in the horizontal direction and the model has 16 vertical layers.

Outside this basin the boundary condition for the atmosphere model is a passive mixed layer, which will be described below. Apart from the reduction in computing time, an advantage of a basin configuration is that the mechanism of air–sea interaction over the Atlantic can be isolated from other processes like the influence of Pacific SST anomalies on the atmospheric circulation over the Atlantic.

The hierarchy of ocean models used in this study consists of a mixed layer model with an increasing number of dynamical processes included:

- horizontal and vertical Ekman transport,
- wind-induced mixing,
- barotropic transport.

1) Passive mixed layer

The first model in the hierarchy is a passive mixed layer model for which the equation of the mixed layer temperature T is given by

$$\frac{\partial T}{\partial t} = -\frac{Q}{h\rho_w c_p} + F_m. \tag{1}$$

Here Q is the net surface heat flux leaving the ocean, h the mixed layer depth, ρ_w the density, c_p the specific heat capacity of seawater, and F_m represents the induced heat transport by the ocean and all other processes neglected by (1). To ensure that the climatology of the mixed layer model stays close to the observed climatology, we computed F_m using (1) from a 50-yr atmosphere-only run with prescribed SSTs:

$$F_m = \frac{\partial T_{\text{clim}}}{\partial t} + \frac{Q_{\text{diag}}}{h\rho_w c_p}, \tag{2}$$

where T_{clim} is the daily mean observed climatological SST computed by linear interpolation from the climatological monthly mean SST of Da Silva et al. (1994), and Q_{diag} is the daily mean diagnosed net surface heat flux; F_m computed by (2) varies in space and goes through an annual cycle.

2) Mixed layer dynamics

Including advection and wind-induced mixing, the equation for the mixed layer becomes

$$\frac{\partial T}{\partial t} = -\frac{1}{h}\left(\frac{Q}{\rho_w c_p} + \mathbf{U}\cdot\boldsymbol{\nabla}_h T + w\Delta T\right) + W + F_r, \tag{3}$$

where $\mathbf{U}$ is the horizontal transport in the mixed layer, $\boldsymbol{\nabla}_h$ is the horizontal part of the gradient operator, and w and ΔT are the vertical velocity and temperature jump at the base of the mixed layer; W is the temperature tendency in the mixed layer due to wind-induced mixing and F_r represents, similar as F_m in (1), all the processes neglected by (3). The advection terms we are considering in this article are Ekman and barotropic transport; that is, $\mathbf{U} = \mathbf{U}_e + \mathbf{U}_b$.

The vertically integrated horizontal Ekman velocity or Ekman transport $\mathbf{U}_e$ is given by

$$\mathbf{U}_e = (U_e, V_e) = \frac{1}{\rho_w(f^2 + r^2)}(f\tau_y + r\tau_x, -f\tau_x + r\tau_y), \tag{4}$$

where f is the Coriolis parameter, τ the wind stress, and r a linear friction term. For $r = 0$, the usual form of Ekman transport is retrieved. Requiring the Ekman transport to be divergence free yields the vertical or Ekman pumping velocity:

$$w_e = \nabla_h \cdot \mathbf{U}_e = \frac{1}{\rho_w(f^2 + r^2)}[f(\nabla \times \boldsymbol{\tau})_z + r\nabla\cdot\boldsymbol{\tau}]. \tag{5}$$

The barotropic transport in the mixed layer $\mathbf{U}_b$ is estimated by solving the Stommel equation for a wind-driven barotropic flow:

$$\kappa_s\nabla^2\psi + \frac{\partial_\phi f}{a^2\cos\phi}\frac{\partial\psi}{\partial\lambda} = \frac{\mathbf{k}\cdot\boldsymbol{\nabla}\times\boldsymbol{\tau}}{\rho_o}, \tag{6}$$

where ψ is the barotropic streamfunction, ϕ latitude, λ longitude, a the radius of the earth, $\mathbf{k}$ the unit vector in the vertical, and κ_s is the linear friction coefficient. When discretized this equation gives a linear set of equations $A\psi = b$, which is solved using a lower upper (LU) decomposition of A. To obtain the barotropic transport in the mixed layer (U_b), the barotropic velocity $\boldsymbol{u}_b$, derived from ψ, is multiplied by the mixed layer depth h.

The wind-induced mixing term W describes the vertical mixing of thermocline waters into the mixed layer due to wind stirring. Especially in the Tropics and subtropics with a warm and shallow mixed layer, this is

potentially an important process. Based on the mixed layer model of Niiler and Kraus (1977), SH estimates the effect of wind-induced mixing on SST to be proportional to the cube of the friction velocity divided by the mixed layer depth,

$$W = -\frac{\alpha}{h} u_*^3, \tag{7}$$

where u_* is the friction velocity, defined by $u_*^2 = \tau/\rho_w$.

Because we are interested in the effect of anomalous wind stress $\hat{\boldsymbol{\tau}} = \boldsymbol{\tau} - \overline{\boldsymbol{\tau}}$ on the mixed layer temperature we rewrite (3) as

$$\frac{\partial T}{\partial t} = -\frac{1}{h}\left(\frac{Q}{\rho_w c_p} + \hat{\mathbf{U}} \cdot \boldsymbol{\nabla}_h T + \hat{w}\Delta T + \alpha \hat{u}_*^3\right) + F_r', \tag{8}$$

where $\hat{\mathbf{U}}$ and $\hat{w}$ are the anomalous transports due to the anomalous wind stress and $\hat{u}_*^3 = u_*^3 - \overline{u}_*^3$. The climatological wind stress $\overline{\boldsymbol{\tau}}$ and $\overline{u}_*^3$ are computed from the 50-yr atmosphere-only run with prescribed SSTs:

$$F_r' = F_r - \frac{1}{h}(\overline{\boldsymbol{U}} \cdot \nabla_h T + \overline{w}\Delta T + \alpha \overline{u}_*^3).$$

By taking the climatological mean of (8) we see that we can estimate F_r' by F_m computed in (2). By doing this we are neglecting the contributions of $\hat{\mathbf{U}} \cdot \boldsymbol{\nabla}_h \hat{T}$ and $\hat{w}\Delta\hat{T}$ to the mean climate, which are considered to be small. The validity of this approach was verified by comparing the climatology of the mixed layer model with the observed SSTs, the differences being in the order of 0.2°C.

3. Results

a. Climatology and variability of SPEEDY forced with climatological SST

To evaluate the quality of the atmospheric circulation simulated by SPEEDY, we performed a 50-yr integration with prescribed climatological SSTs. We will focus here on the circulation over the South Atlantic. A more extensive evaluation of the climatology of SPEEDY can be found in Molteni (2003). Figure 1 shows the annual MSLP and the dominant empirical orthogonal functions (EOFs) of MSLP for 3-month seasonal mean averages from which the annual cycle is subtracted. For comparison the climatology of the NCEP–NCAR reanalysis is also shown. The climatology of SPEEDY compares well with the NCEP–NCAR reanalysis, although the intensity of the subtropical high is somewhat overestimated. Also, the structure and explained variance of the first two EOFs of MSLP are in good agreement with the modes obtained by SH from the NCEP–NCAR reanalysis (Fig. 2 of SH). These results indicate that SPEEDY can be used as a reliable tool for simulating the dominant patterns of variability over the South Atlantic.

The good correspondence between the simulated and observed EOFs of MSLP, when SPEEDY is forced with climatological SSTs, is also indicative of the fact that the structure of the dominant modes of variability in the atmosphere is mainly due to atmospheric dynamics. This agrees with the accepted knowledge of atmospheric variability outside the Tropics (Corti et al. 1999; Haarsma and Selten 2001).

b. SPEEDY–MICOM

To check if, indeed, the fully coupled model is able to simulate the dominant modes of coupled variability, we integrated SPEEDY–MICOM for 60 yr from which we used the last 40 yr for the analysis. Figure 2 displays the first two singular value decomposition (SVD) modes of MSLP and SST for 3-month seasonal averages from which the annual cycle is subtracted. The time series of the principal components (PCs) are normalized with respect to their standard deviation so that the patterns indicate the characteristic amplitude of the mode of variability. The first SVD mode displays for the MSLP a monopole, which is reminiscent of the first EOF of the MSLP (Fig. 1), although the pattern is more extended in the equatorward direction. The dominance of the first EOF in this pattern is confirmed by the strong correlation between the time series of the EOF and SVD pattern of MSLP (0.93). The SST pattern shows a predominantly southwest–northeast oriented dipole. This SVD mode shows a strong resemblance in pattern and explained variance with the first SVD mode of SH (their Fig. 3), which was computed from NCEP–NCAR reanalysis data. The SST pattern also compares favorably with the dominant EOF computed by Palastanga et al. (2002).

The agreement with the second SVD mode of SH (their Fig. 3) is less. The MSLP dipole pattern of this mode shows good agreement, but the SST pattern lacks the tripole structure of the mode computed by SH. The second SVD mode is, according to SH, related to El Niño variability. Because outside the Atlantic basin the ocean in SPEEDY–MICOM is represented by a passive mixed layer, the model does not simulate an El Niño type of variability. This might explain the difference between the simulated second SVD and the observed one as computed by SH. In addition, it may be noted that there is also a large difference in the second SVD mode between SH and Venegas et al. (1997).

As a consequence of the foregoing discussion, we will in the rest of this paper concentrate on the first SVD mode, which explains by far most of the variance, in the order of 33%, compared to 24% for the second SVD

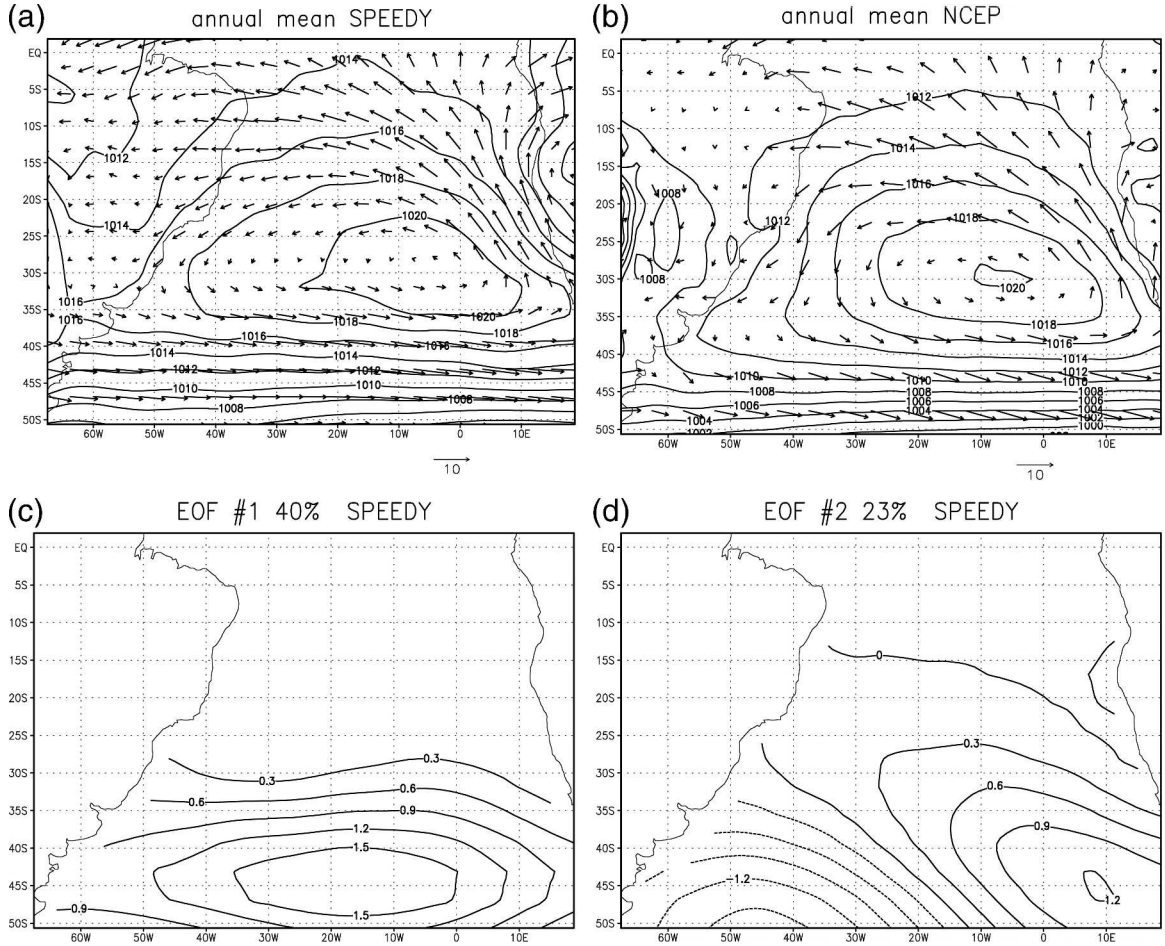

FIG. 1. Annual mean MSLP (hPa) and near-surface winds (m s^{-1}) (a) simulated by SPEEDY with prescribed climatological SSTs and (b) obtained from the NCEP–NCAR reanalysis. (c), (d) The first two EOFs of MSLP simulated by SPEEDY for 3-month seasonal mean averages from which the annual cycle is subtracted.

mode. The explained variance of the first SVD mode is in accordance with the value obtained by SH (38%). The ability of SPEEDY–MICOM to simulate the observed dominant mode of variability demonstrates that this model configuration contains the essential physics for generating these patterns. Using the hierarchy of ocean models described in section 2, we will in the remainder of this paper investigate what are the dominant mechanisms for generating these patterns of coupled variability.

c. Passive mixed layer

In our first experiment, we used a constant mixed layer depth of 80 m, which is a reasonable mean value for the South Atlantic Ocean between 50°S and the equator. The horizontal resolution is the same as the atmosphere model, that is, 3.75°. The time step of the passive mixed layer model is 1 day. A 120-yr integration of the atmosphere model coupled to the passive mixed layer described by (1) was executed, of which the last 100 yr were analyzed. The differences in the entire global ocean between the 100-yr-averaged seasonal mean mixed layer temperatures and the observed climatological seasonal mean SSTs are in the order of 0.5°C, with maximum differences along the sea–ice margin. The results shown below are for 3-month seasonal means from which the annual cycle is subtracted.

Figure 3 displays for the South Atlantic the first SVD mode of MSLP and SST. Similar to the SPEEDY–MICOM simulation, the first SVD shows a dipole pattern for the SST and a monopole for the MSLP. The pattern correlations with the first SVD of SPEEDY–MICOM are 0.82 and 0.67 for MSLP and SST, respectively. Also, the amplitude and the explained variance of these patterns are close to those of the SPEEDY–

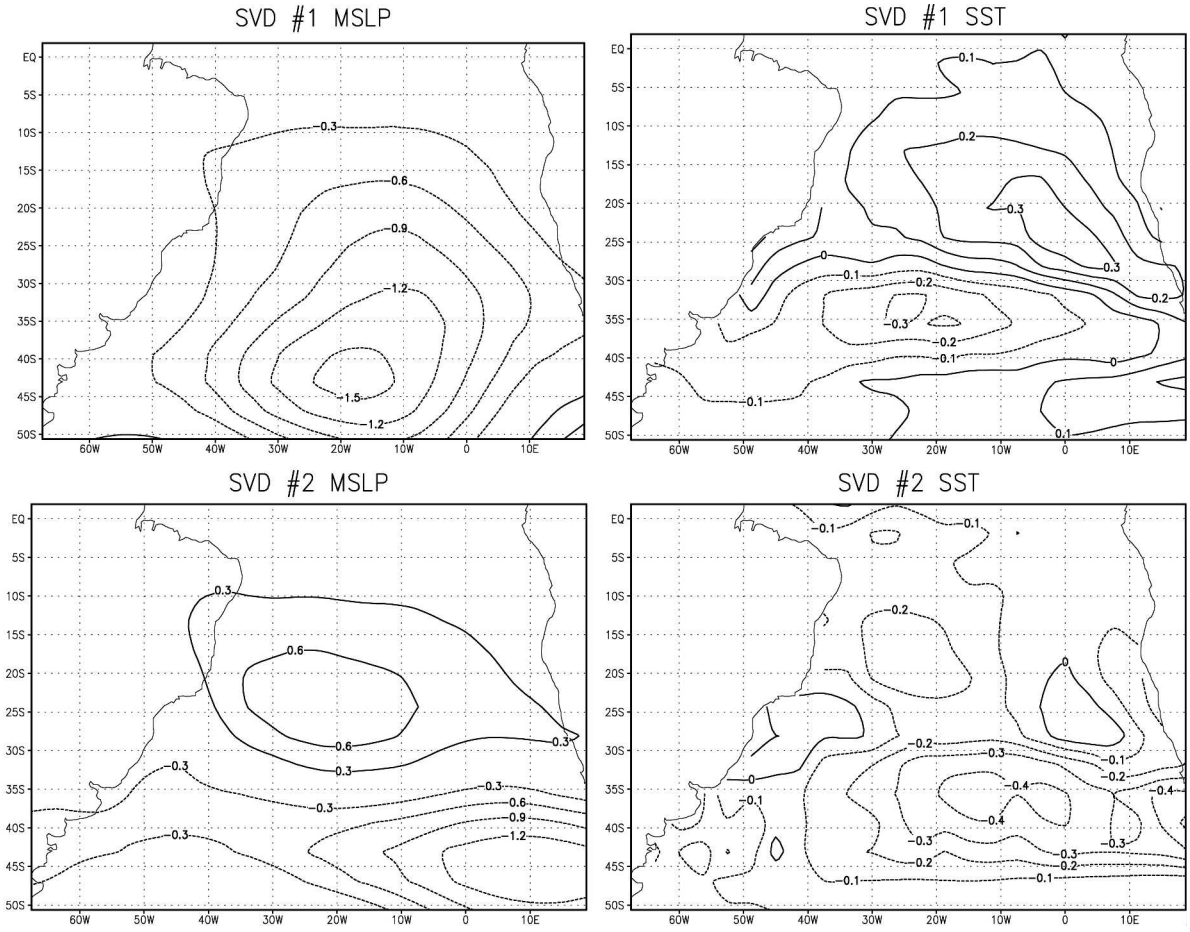

FIG. 2. First two leading modes of a combined SVD analysis of MSLP (hPa) and SST (K) anomalies for the SPEEDY–MICOM run. The spatial patterns are scaled such that the values correspond to one standard deviation. The modes account for 33% and 24%, respectively, of the total squared variance.

MICOM run. The main heat source for generating the SST anomalies is the latent heat flux (LHF), whereas the sensible heat flux (SHF) and radiation terms are less important. The first SVD between MSLP and LHF (not shown) displays the same pattern as for MSLP and SST. Comparison of the MSLP pattern of the SVD with the climatological MSLP pattern (Fig. 1a) reveals that variation of this pattern enhances or reduces the climatological trade winds at the equatorward pole of the SST dipole. At the poleward pole it predominantly induces anomalous meridional advection. From this we conclude that the equatorward pole of the SST dipole is caused by enhancement or decrease of the climatological trade winds, which consequently enhance or diminish the latent heat flux, whereas the poleward pole is caused by anomalous meridional advection of climatological surface air temperatures (SATs).

Notwithstanding the similarity, a closer inspection of the SVD patterns of MSLP and SST reveals significant differences with those of SPEEDY–MICOM. The MSLP pattern is shifted 10° equatorward and shows no clear resemblance with the first EOF MSLP mode, as was the case in SPEEDY–MICOM and also noticed by SH. The correlation between the time series of the EOF and the SVD pattern of MSLP is less (0.73) than in the SPEEDY–MICOM run (0.93). In accordance with the equatorward shift of the MSLP pattern, the SST dipole is also shifted equatorward. In addition, the zonal extent of the poleward maximum of the SST dipole is less, displaying a more circular structure. These differences clearly demonstrate the active role of the ocean in generating the SST anomalies and thereby the dominant patterns of coupled variability.

d. Ekman transport

As a first step to evaluate the role of ocean dynamics, the anomalous Ekman transport terms were included in

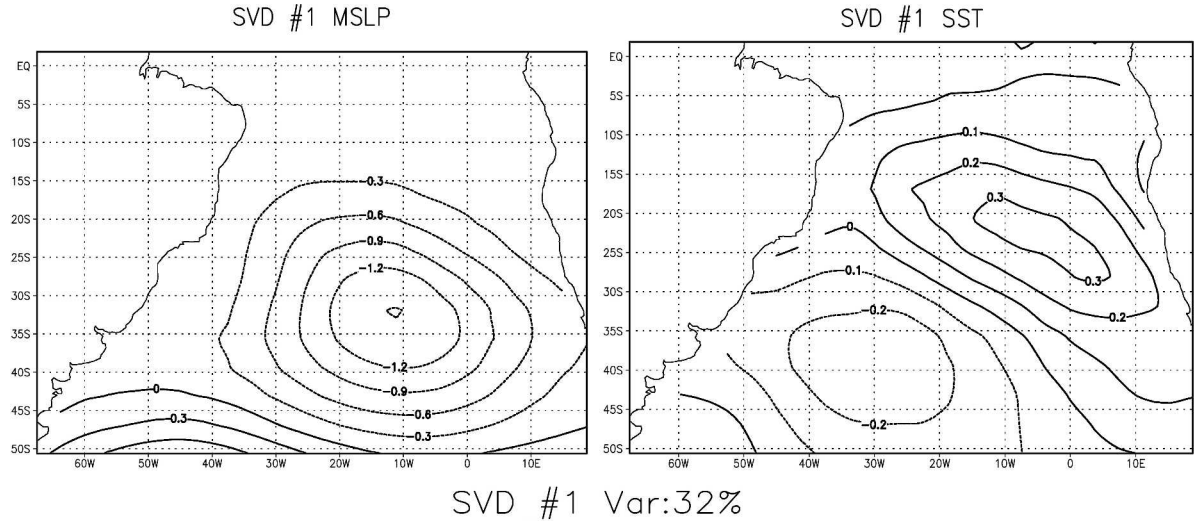

FIG. 3. The leading mode of a combined SVD analysis of MSLP (hPa) and SST (K) anomalies for the SPEEDY-passive mixed layer run. The spatial patterns are scaled such that the values correspond to one standard deviation. The explained total squared variance is 32%.

the mixed layer model (8): $\hat{\mathbf{U}} = \hat{\mathbf{U}}_e$ and $\hat{w} = \hat{w}_e$, where $\hat{\mathbf{U}}_e$ and $\hat{w}_e$ are given by (4) and (5), respectively. The anomalous wind-induced mixing $-(\alpha/h)\hat{u}_*^3$ is set to zero.

For the numerical evaluation of the advection terms in (8), this equation is rewritten in flux form and discretized on an Arakawa-B grid. A leapfrog scheme with a time step of 1 day is used for the time integration.

For the temperature jump across the mixed layer, ΔT in (8), we chose a value of 2 K, which is, as SH argued, a reasonable value for the South Atlantic. For the linear friction r in (4) we used a value of $r = 2.5$ day^{-1}. This value is small enough to be negligible away from the equator but large enough to avoid singularity. Similar as for the passive mixed layer, a 120-yr integration was performed of which the last 100 yr were analyzed.

The SVD analysis of MSLP and SST revealed for the first mode a significant difference compared with the passive mixed layer without Ekman transport. Most notably, the southern pole of the SST dipole pattern shows a much more elongated structure in agreement with the fully coupled model and observations. However, the amplitude of this poleward pole seems to be overestimated, whereas the amplitude of the equatorward pole is reduced and is smaller than simulated by SPEEDY–MICOM. A regression analysis between the PC of the MSLP pattern of the SVD analysis onto the Ekman transport terms in (8) reveals a zonally elongated monopole at 40°S, demonstrating that the effect of Ekman transport on SST variability is mainly confined to the latitude belt south of 30°S. The largest contribution to the Ekman transport terms comes from the anomalous meridional advection of climatological SST by anomalous meridional Ekman velocity caused by anomalous zonal winds. Anomalous winds and climatological SST gradients are strongest in the southern part of the basin, explaining the dominance of the Ekman transport term there. Comparison between the tendency terms in (8) due to horizontal Ekman transport and Ekman pumping revealed that the latter term in that region is about a factor of 4 smaller.

Although for the entire South Atlantic a mixed layer depth of 80 m is a reasonable estimate, a more detailed analysis of the Levitus and Boyer (1994) data as well as the SPEEDY–MICOM data reveals that south of 40°S a mixed layer depth of 200 m is a more appropriate estimate, whereas north of 30°S the mixed layer depth is close to 50 m. We therefore performed a new experiment with a variable mixed layer depth using these estimates. Between 30° and 40°S the mixed layer depth is linearly interpolated between 50 and 200 m.

The combined SVD analysis of MSLP and SST for the experiment with the variable mixed layer depth reveals that the patterns of MSLP and SST of the first SVD mode are now approximately located at the right position and have the right orientation. Also, the amplitude and explained variance are now more in agreement with the SPEEDY–MICOM run. The spatial correlations of the MSLP and SST pattern with those of SPEEDY–MICOM are 0.89 and 0.78, respectively, showing a marked increase from the passive mixed layer experiment (0.82 and 0.67). The correlation between the time series of the EOF and the SVD pattern has increased from 0.73 to 0.85, implying an increase in

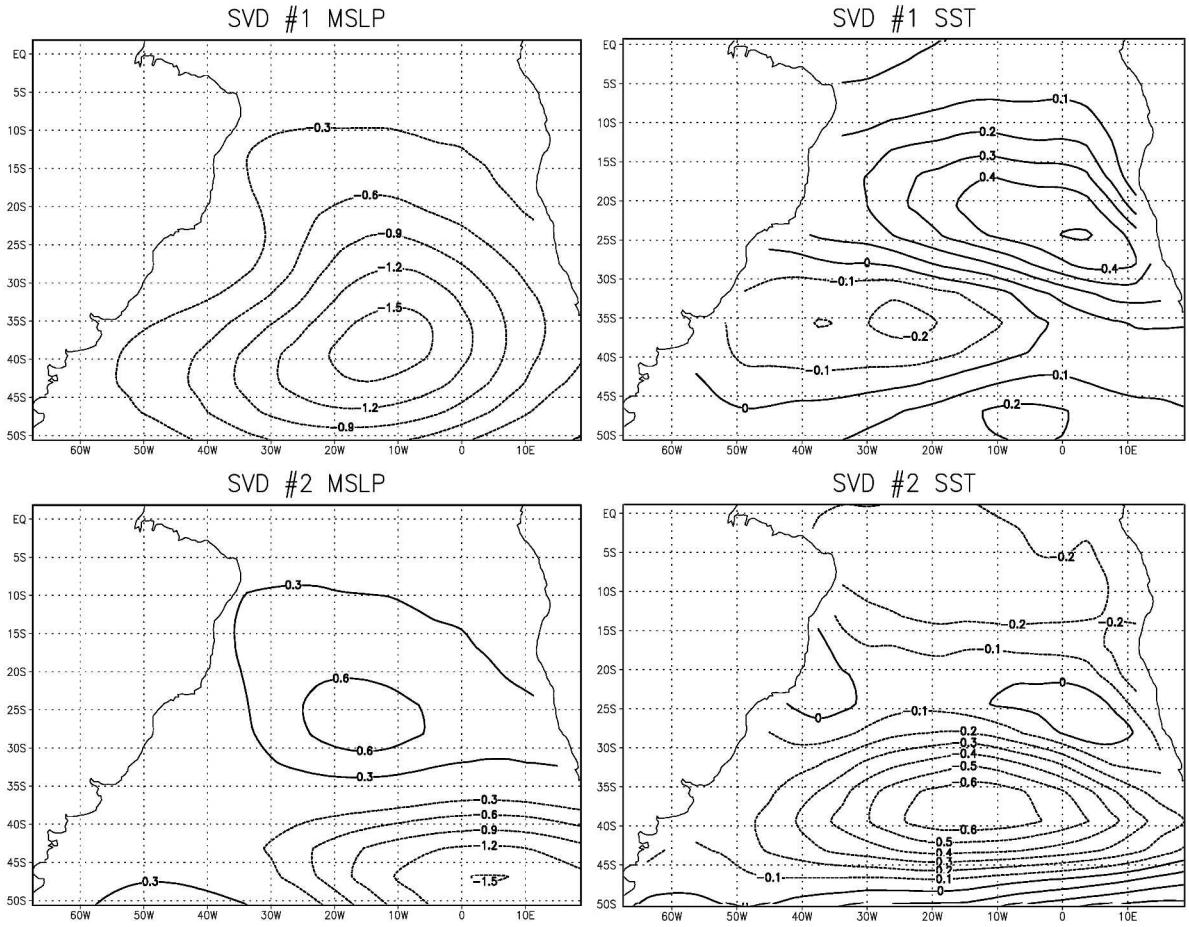

FIG. 4. As in Fig. 2 but for the run with Ekman transport and wind-induced mixing with a variable mixed layer depth. The explained total squared variances for these modes are 30% and 27%, respectively.

the explained variance from 53% to 72% with respect to the passive mixed layer experiment and is now more close to the value of the SPEEDY–MICOM run (0.93).

Although the Ekman transport term seems to be important for a realistic simulation of SST variability, one can ask how much of the improvement of the simulated SVD pattern, compared to the passive layer experiment, is due to a more realistic estimation of the mixed layer depth. We therefore repeated the passive mixed layer experiment with the same estimation of the latitudinally varying mixed layer depth. The SVD analysis shows that the poleward pole of the SST dipole is now severely underestimated, as a consequence of the deep mixed layer, revealing the importance of the Ekman transport term for the generation of SST variability south of 30°.

e. Wind-induced mixing

From their analysis of NCEP–NCAR data, SH argue that wind-induced mixing is crucial for generating the dominant patterns of coupled variability. The factor α in (7) is estimated in SH by 20 K s^2 m^{-2}. The exact value of this factor is, as SH pointed out, rather uncertain. The chosen value gives only an estimation of the order of magnitude.

Because of the unavailability of 6-hourly data, SH derived u_*^3 from monthly mean data. This means that in their computations the effect of wind-induced mixing is underestimated. Analyzing the difference between the climatological u_*^3 resulting from the different ways of computing, it appeared that by using monthly mean data in the central South Atlantic u_*^3 is generally underestimated by a factor of 1.5. In the southern part of the basin the difference is larger, in the order of a factor of 4. The deep mixed layer south of 40°S also diminishes the effect of wind-induced mixing on the mixed layer temperature. Taking these arguments in consideration, we chose a value of 10 K s^2 m^{-2} for α.

Figure 4 shows the SVD analysis between MSLP and SST. Comparison with the SVD modes of SPEEDY–

MICOM reveals that the first mode is now almost perfectly simulated. Compared to the mode obtained in the experiment without wind-induced mixing, most notably for the SST pattern, is the shift of the maximum of the equatorward pole to the southeast corner of the basin and the confinement of the poleward pole to the latitude belt between 30° and 45°S. The tilt of the MSLP pattern changed from southeast–northwest to southwest–northeast in according with the SPEEDY–MICOM simulation. Although we are primarily interested in the first SVD mode, Fig. 4b shows that the second SVD mode is also in close agreement with the second SVD mode of SPEEDY–MICOM (Fig. 2b). It displays a meridional MSLP dipole in the southeast–northwest direction and a large SST band along approximately 35°S, although the SST values are somewhat overestimated. This demonstrates that the processes in MICOM responsible for the generation of the dominant modes of coupled MSLP–SST variability are well captured by (8), where the anomalous velocities are due to Ekman transport.

To investigate in more detail the relative contribution of the wind-induced mixing term and its relation to the other forcing terms, we computed the regression of the PC of the MSLP pattern of the SVD analysis of MSLP and SST onto the different forcing terms. The results are shown in Fig. 5. The regression pattern for the wind-induced mixing shows a tripole pattern. This pattern can be understood by noting that the MSLP pattern of the SVD analysis is not merely an amplification or reduction of the climatological mean (cf. Figs. 4a and 1a), but also implies a shift in the position and orientation of principally the trade winds. This causes the northern dipole: the wind-induced mixing is less where the trade winds are weakened and vice versa. Between 45° and 50°S the MSLP pattern results in a change in the strength of the westerlies, which is the cause of the most poleward pole of the tripole structure of the wind-induced mixing term.

Comparing the three terms in Fig. 5 we see that for the equatorward pole the surface flux is the dominant term except for the southeastern corner, whereas for the poleward pole all three terms seem to be important for the correct simulation. There appears to be a partial cancellation between the Ekman transport and the wind-induced mixing terms.

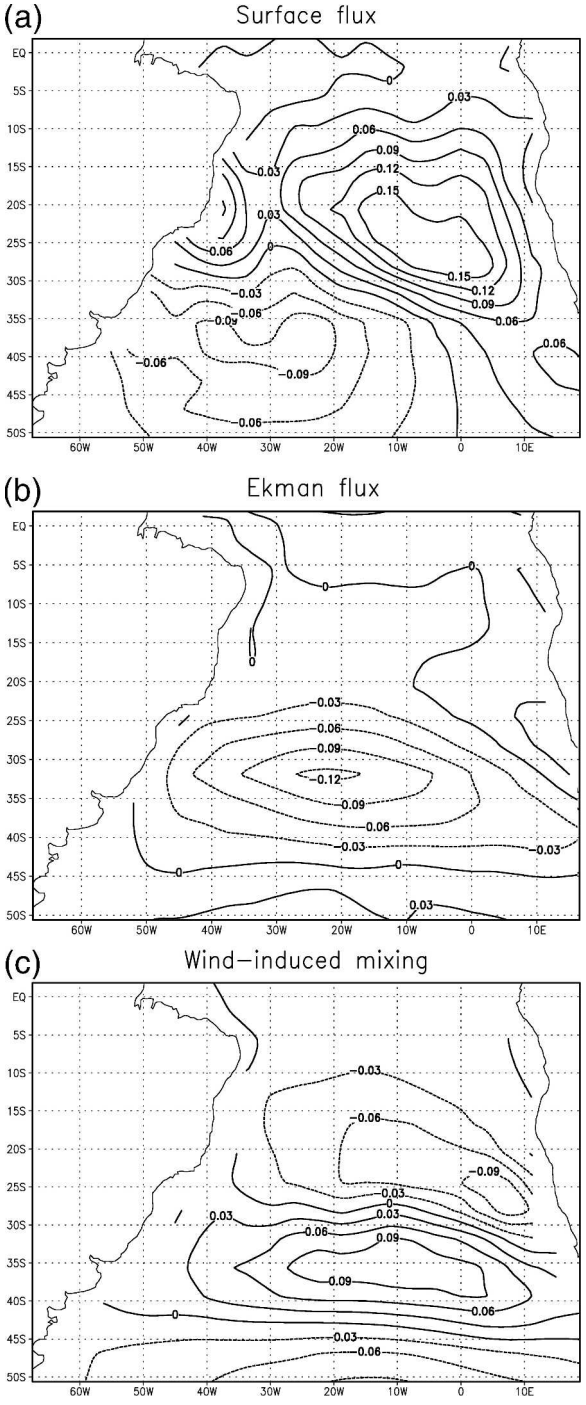

FIG. 5. Regression of the PC of MSLP of the first MSLP–SST SVD mode onto the different terms in the tendency equation: (a) surface flux, (b) Ekman transport, and (c) wind-induced mixing. The units are in kelvin (3 month)$^{-1}$.

f. Barotropic transport

Although the foregoing results indicate that latent heat flux, Ekman transport, and wind-induced mixing are the most important terms in generating the dominant patterns of coupled ocean–atmosphere variability, advection by wind-driven barotropic currents might be important in specific areas. Especially in regions of strong boundary currents and large SST gradients barotropic transport might play an important role. In the

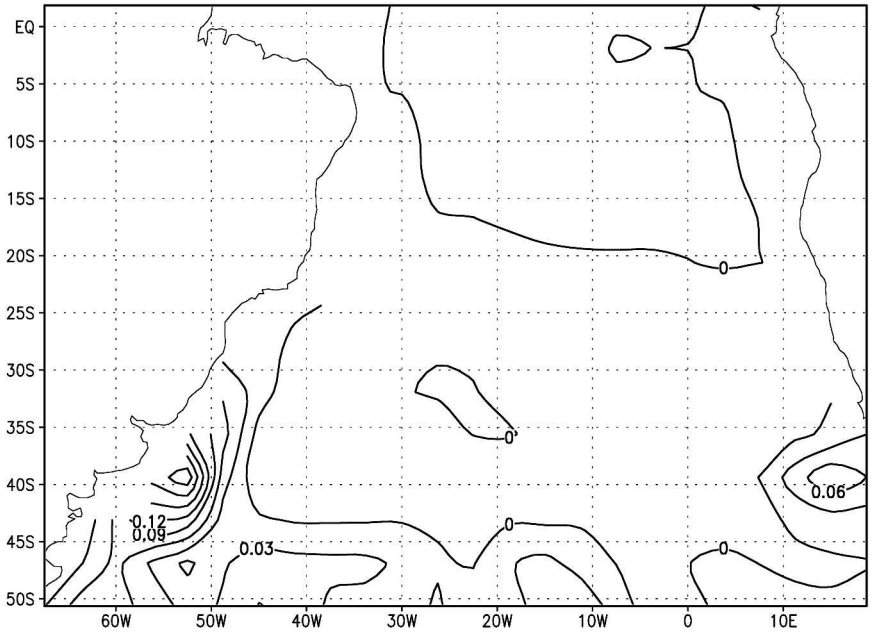

FIG. 6. Regression of the PC of the first EOF mode of MSLP onto the barotropic transport term in the tendency equation (8) for the SST. The units are in kelvin (3 month)$^{-1}$.

Atlantic basin a region where these conditions exist is the Brazil–Malvinas confluence zone.

To investigate this, we added in (8) the effect of the advection by the anomalous barotropic transport circulation computed by (6): $\hat{\mathbf{U}} = \hat{\mathbf{U}}_e + \hat{\mathbf{U}}_b$. For the linear friction coefficient κ_s, we chose a value of 4×10^{-6} s^{-1}.

The annual mean barotropic streamfunction resulting from the climatological SPEEDY wind stress computed by (6) for the South Atlantic Ocean is a subtropical gyre of 12 Sv (Sv $\equiv 10^6$ m^3 s^{-1}). This is about half of the intensity of the subtropical gyre simulated by MICOM in the coupled run. Although the Stommel equation at this coarse resolution of 3.75° only gives a first-order estimate of the barotropic wind-driven currents, it may help us get an indication of the importance of the anomalous advection by barotropic currents for the generation of SST anomalies. To compute the upper horizontal barotropic transport we have to assume a scale depth. Using a scale depth of 500 m gave a reasonable estimate of the barotropic transport compared to MICOM. Figure 6 shows the regression of the first EOF of MSLP onto the barotropic transport term in the tendency equation for the SST [(8)]. It reveals that, indeed, apart from the regions of the Malvinas–Brazil confluence zone and at the South African coast, the effect of the anomalous barotropic circulation on the seasonal mean SST anomalies is small. An SVD analysis between MSLP and SST shows only minor differences with respect to the experiment without the barotropic term included. The Stommel equation (6) describes the steady-state solution of the barotropic wind-driven circulation after the adjustment of barotropic Rossby waves. The analyses are done for seasonal means, which may be too short for the adjustment process. We therefore repeated the calculations using annual mean averaged wind stresses for calculating the barotropic transport. The results are basically the same. The recalculation of the regression of the first EOF of MSLP onto the barotropic transport term in the tendency equation for the SST reveals a figure very similar to Fig. 6. The main difference is a reduction in amplitude of about 50%, which is to be expected owing to smaller annual mean wind stress anomalies compared to seasonal mean anomalies. From this we conclude that the effect of the wind-driven barotropic currents on SST variability is only significant in these localized regions, having the largest impact in the Brazil–Malvinas confluence zone. In the Brazil–Malvinas confluence zone large SST gradients exist. Small changes in the in the boundary currents due to anomalous wind forcing can therefore easily generate large SST anomalies. A sensitivity analysis of SST variability due to the wind-driven barotropic currents is, however, outside the scope of this study and requires a much more careful simulation of the wind-driven circulation than the Stommel equation (6).

4. Budget analysis of SST variability

To obtain a more quantitative picture of the relative contribution of the different terms to the dominant pat-

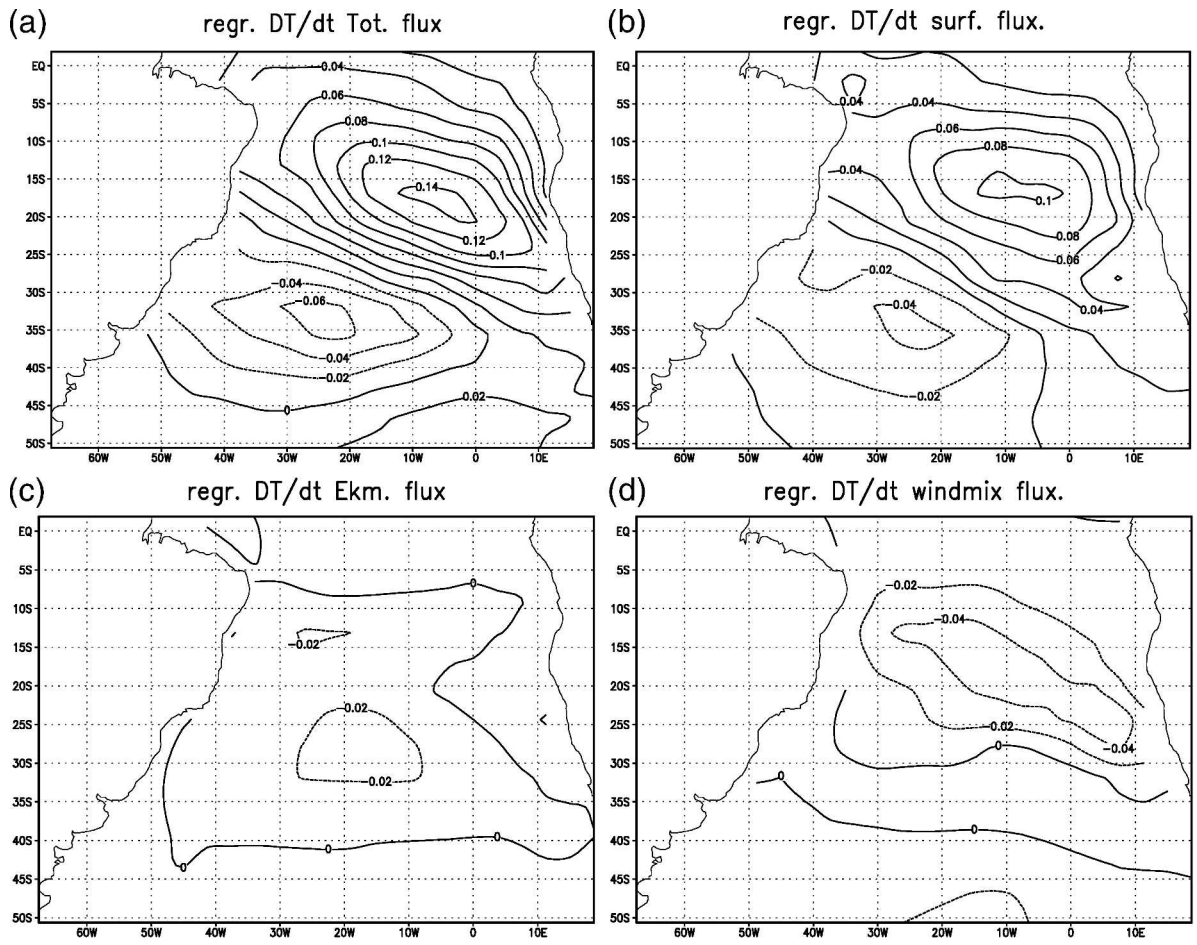

FIG. 7. Regression of the SST tendency onto the different terms in the tendency equation: (a) total heat flux, (b) surface flux, (c) Ekman transport, and (d) wind-induced mixing. The units are in kelvin (3 month)$^{-1}$.

terns of SST variability, we tried to estimate the contribution of the different terms in (8) to the structure of the SST pattern of the SVD analysis of MSLP and SST. Because, as discussed in the foregoing section, the wind-driven currents only affect SST variability in localized regions, we will concentrate here on the surface heat flux, Ekman transport, and wind-induced mixing terms. We performed a regression analysis of the time derivative of the principal component of this SST pattern on the different terms in (8). The result is shown in Fig. 7. The main contribution is from the net surface heat flux, which is dominated by the latent heat flux. The contribution from the Ekman transport and the wind-induced mixing terms is much less. The small value of the Ekman transport term might be surprising in light of the results in section 3d. However, the Ekman transport term attains its maximum amplitude between 25° and 30°S where the surface flux changes sign and is about zero. In addition, as discussed in section 3d, with the inclusion of the Ekman transport terms the MSLP pattern of the SVD analysis changes in position and structure with respect to the experiment when only the surface fluxes are included (section 3c). This means that the surface flux term in Fig. 7 already bears the influence of the Ekman transport term.

This analysis is consistent with the results obtained by SH, who concluded from a similar analysis that the Ekman transport is of minor importance. Using a model hierarchy, however, we demonstrated that despite its rather small value the Ekman transport term is significant in modifying the shape of dominant SVD patterns.

5. Time evolution

a. Spectral analysis

The spectra of the PCs of SST in the SVD analysis of MSLP and SST for SPEEDY–MICOM and for the mixed layer model including Ekman transport and wind-induced mixing are shown in Fig. 8. Neither of the

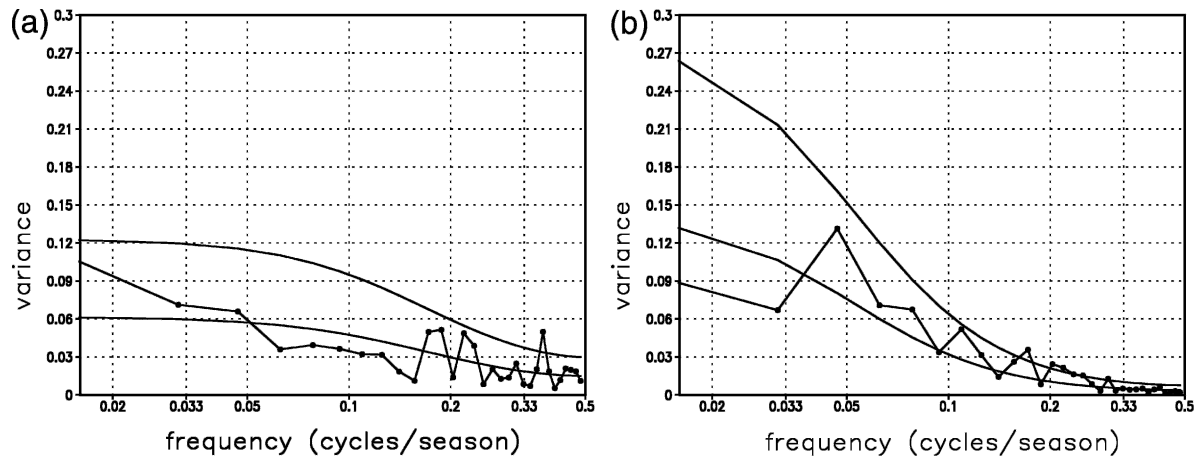

FIG. 8. Spectra of the PCs of the SST patterns of the first SVD of MSLP and SST together with the fitted AR(1) (red noise) process spectrum and the 95% a priori confidence level for (a) SPEEDY–MICOM and (b) SPEEDY coupled to the mixed layer model with Ekman transport and wind-induced mixing.

two spectra shows a clearly dominant time scale. The most striking aspect is that the spectrum for SPEEDY coupled to the mixed layer model is significantly more red than for SPEEDY–MICOM. For time scales greater than 5 yr the variance is enhanced by more than 50%. The reddening also occurs for the time series of SST anomalies at individual grid points. Investigation of the other mixed layer models used in this study revealed that the reddening occurred all in models.

The reddening of the SST spectra for an atmosphere model coupled to an ocean mixed layer model compared to a fully coupled atmosphere–ocean model was discussed by Drijfhout et al. (2001) and explained by the too strong coupling of SST anomalies to SAT anomalies in the absence of ocean dynamics. There it was demonstrated that ocean advection, creating patterns of SST variability that do not match the preferred modes of SAT variability, is the main cause for the damping of SST anomalies. Because the mixed layer models used in this study do not simulate the advection by the mean currents [(8)], the argument of Drijfhout et al. is also valid here. There the reddening for the globally averaged spectra was about 20%, which is less than the reddening observed in this study. This difference can be due to the different atmosphere and ocean models used in this study. Also the reddening estimated in Drijfhout et al. is a globally averaged value.

The spectra of the PCs of the MSLP patterns of the SVD analysis are white, without a dominant time scale for all models. No significant reddening of the MSLP spectra is observed for SPEEDY coupled to the mixed layer models.

The absence of a clearly dominant time scale in SPEEDY–MICOM might be due to the relatively short time integration (40 yr) used in this study, which hampers the detection of a weak signal. It may also be due to the absence of the necessary processes for generating this time scale. For instance, as stated before, in SPEEDY–MICOM no ENSO variability is simulated because, outside the South Atlantic basin, the ocean is represented by a passive mixed layer. Therefore, the influence of ENSO on interannual and decadal time scales on the South Atlantic climate (Mo and Häkkinen 2001) cannot be modeled. Also, low-frequency variability in the South Atlantic related to changes in the thermohaline circulation driven by changes in the deep-water formation as suggested by Latif (2001) and other studies cannot be adequately simulated by the regional ocean model.

b. *Propagation of patterns*

The lack of a dominant time scale in the spectra of the PCs of SST and SVD of the dominant SVD modes does not suggest the existence of propagating signals related to periodic behavior. An extended EOF analysis of SST anomalies confirmed this. No statistically significant propagating patterns could be found.

The equatorward center of the SST dipole of the first SVD is located in a ventilation area. Lazar et al. (2001) have shown for an ocean model coupled to an advective atmosphere mixed layer model (Seager et al. 1995) that an SST anomaly in that region will be subducted and moved in the northwesterly direction toward the north Brazilian coast. Here we investigated whether in a fully coupled atmosphere–ocean model, like SPEEDY–MICOM, the subduction and subsequent advection of SST anomalies can also be detected.

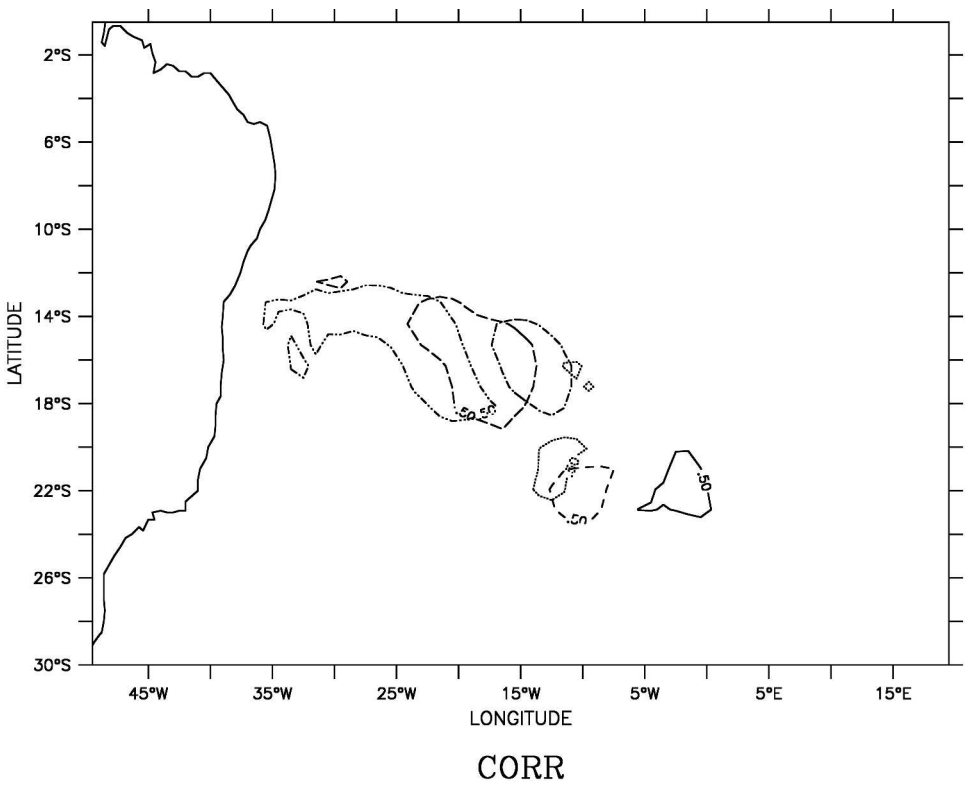

FIG. 9. The 0.5 contour (solid line) of the correlation of the winter (JJA) SST anomalies averaged over the region 25°–20°S, 10°W–0°, with the thickness anomalies in the $\sigma = 26.18$ layer in the following summer (Dec–Jan–Feb). The 0.5 contours of the lag correlation of summer thickness anomalies in this region with summer thickness anomalies at subsequent years: year 1 (dashed), year 2 (dotted), year 3 (dashed–dotted), year 4 (long dashed), and year 5 (dashed–dotted–dotted).

The subduction process is tied to the annual cycle. At the end of the austral winter [June–July–August (JJA)], the mixed layer restratifies, leaving the temperature anomaly in the layers below the mixed layer. When at the beginning of the following winter the mixed layer entrains, part of the temperature anomalies of the previous winter reemerges in the mixed layer. However, a significant part of that temperature anomaly has been subducted and advected away and will not reenter the mixed layer. Figure 9 shows the 0.5 contour of the correlation of the winter SST anomalies averaged over the region 25°–20°S, 10°W–0°, which is located in the equatorward pole of the SST dipole, with the thickness anomalies in the $\sigma = 26.18$ layer in the following summer (DJF) when the mixed layer is detrained. The subsequent movement of these thickness anomalies in the $\sigma = 26.18$ layer is indicated by the displacement of the 0.5 contour of the lag correlation of this thickness anomaly with thickness anomalies at subsequent years. It shows that in about 6 yr the anomalies cross the South Atlantic reaching the coast of north Brazil, in agreement with the results of Lazar et al. (2001). Because of the limited length of the integration and the diffusive spreading of the anomalies, we are not able to make firm statements about the fate of the anomaly when it reaches the Brazilian coast. The results from Lazar et al. (2001) suggest that it is advected northward by the North Brazilian Undercurrent and finally is spread along the equator.

In SPEEDY–MICOM, the isopycnal layers $\sigma = 25.28$, $\sigma = 25.77$, and $\sigma = 26.18$ all outcrop in that region. Analysis of the subduction in the other two σ layers and of temperature anomalies instead of thickness anomalies revealed similar results. This subduction of SST anomalies enforces the argument of Drijfhout et al. (2001), explaining the reddening of the SST spectra in mixed layer models because it acts as an additional damping of SST anomalies, which is not simulated by the mixed layer models used in this study.

A similar lag correlation analysis of the SST anomalies averaged over the same region, 25°–20°S, 10°W–0° with SST anomalies in the rest of the South Atlantic basin does not reveal significant correlations for lags longer than 2 yr. After this period the SST anomalies

generated by the atmosphere mask the advection by the ocean currents.

6. Conclusions and discussion

Using an atmosphere model of intermediate complexity coupled to an hierarchy of ocean models, we have investigated the physical mechanisms responsible for the dominant patterns of coupled MSLP and SST variability. The results indicate that the patterns are due to a combined effect of turbulent surface heat fluxes, Ekman transport, and wind-induced mixing. The variation in the wind-driven barotropic transport mainly affects the SST variability in the Brazil–Malvinas confluence zone. These results confirm to a large extend those of SH obtained from NCEP–NCAR reanalysis data. The main difference is the role of the Ekman transport terms, which they considered to be of minor importance.

The spectra of the mixed layer models appeared to be too red in comparison with the fully coupled SPEEDY–MICOM model due to the too strong coupling between SST and SAT, resulting from the inability to advect and subduct SST anomalies by the mixed layer models. In SPEEDY–MICOM anomalies in the southeastern corner of the South Atlantic are subducted and advected toward the north Brazilian coast on a time scale of about 6 yr.

Cayan (1992) showed for the North Atlantic and North Pacific that turbulent heat fluxes are the dominant cause for the observed structures of interannual and decadal variability. Our results and those of SH for the South Atlantic indicate that, although the largest contribution to SST variability also comes from the turbulent heat fluxes, the other contributions cannot be neglected.

We speculate that the dominant role of turbulent heat fluxes in the Northern Hemisphere is due to the existence of large continents, which causes a large annual cycle in SST and surface fluxes. The interannual SST anomalies in the Northern Hemisphere are mainly formed during boreal winter, especially at the western boundaries of the ocean. This region is exposed to strong variability in cold air outbreaks from the continent causing large turbulent surface heat fluxes. The deep buoyancy-driven mixed layer diminishes the effect of wind-induced mixing and Ekman transport.

Wainer and Venegas (2002) showed for a coupled climate model that multidecadal variability in the southern South Atlantic is related to variations in the Malvinas western boundary current. We found only a moderate effect of the wind-driven barotropic circulation. The difference can be explained by the different time scales. Our patterns are dominated by interannual-to-decadal variability, whereas the patterns analyzed by Wainer and Venegas (2002) are characterized by multidecadal variability.

Several studies (SH; Mo and Häkkinen 2001) have indicated the influence of El Niño on the climate of South America and the South Atlantic. Owing to the setup of our experiments, in which the Pacific Ocean is modeled by a passive mixed layer, this effect is omitted in our experiments. Sterl and Hazeleger (2003) found that the second SVD mode is significantly correlated with the Niño-3 index. This relationship might be the cause of the differences between the second SVD mode simlulated by the SPEEDY–MICOM model and the one obtained by SH from the NCEP–NCAR reanalysis, although of course we cannot discard the possibility that it is due to some deficiency of the SPEEDY–MICOM model. In any case, the strong correspondence between the first two dominant modes of variability of SPEEDY–MICOM and SPEEDY coupled to the mixed layer model including Ekman transport and wind-induced mixing indicates that the mixed layer model contains the essential physics of MICOM for simulating the dominant SST anomaly patterns.

The reason for this success is that, outside the Tropics on interseasonal and interannual time scales, the dominant interaction is the forcing of the ocean by the atmosphere. The dominant atmospheric modes on these time scales are standing modes with a white spectrum. The dominant EOFs of MSLP for SPEEDY–MICOM and SPEEDY coupled to the mixed layer models have the same structure as the EOFs shown in Fig. 1 for SPEEDY with prescribed climatological SSTs. Analyses of these time series reveal in all cases a white spectrum without a dominant time scale. These atmospheric modes generate an imprint on the ocean mixed layer.

Although most of the atmospheric variability is generated by internal atmospheric dynamics, it is significantly affected by SST variability. The response of the atmosphere to the SST dipole of the SVD analysis is investigated by Haarsma et al. (2003). In this study, the SST dipole of the first SVD shown in Fig. 2 was applied as a lower boundary for SPEEDY, which outside this dipole was forced with prescribed climatological SSTs. The main response of this dipole is a deep baroclinic response northwest of the equatorward pole of the SST anomaly dipole and a shallow equivalent barotropic response over the poleward pole of the SST anomaly dipole. The baroclinic response is strongest during the austral summer and is similar to the response to tropical SST anomalies described by Robertson et al. (2003). The effect of this atmospheric response on the time

evolution of the coupled variability is the subject of ongoing research.

Acknowledgments. This research was supported by FAPESP (Grant 00/04673-0 and 01/10969-6), by CNPq (Proc. 522456/95-2), and by the Inter-American Institute for Global Change Research (IAI) Project SACC/CRN-061. We thank Pedro L. Silva Dias for the stimulating discussions and for his contribution to the initiation of this project. We also thank two anonymous reviewers for their critical and stimulating remarks.

REFERENCES

Barreiro, M., P. Chang, and R. Saravanan, 2002: Variability of the South Atlantic convergence zone simulated by an atmospheric general circulation model. *J. Climate,* **15,** 745–763.

Bleck, R., R. C. Rooth, D. Hu, and L. T. Smith, 1992: Salinity-driven thermocline transients in a wind- and thermohaline-forced isopycnic coordinate model of the North Atlantic. *J. Phys. Oceanogr.,* **22,** 1486–1505.

Cardoso, A., 2001: SST influence on the winter climate of the metropolitan region of São Paulo. M.S. dissertation, Institute of Astronomy and Geophysics, University of São Paulo, 112 pp.

Carton, J. A., X. Cao, B. S. Giese, and A. M. da Silva, 1996: Decadal and interannual SST variability in the tropical Atlantic Ocean. *J. Phys. Oceanogr.,* **26,** 1165–1175.

Cayan, D. R., 1992: Latent and sensible heat flux anomalies over the northern oceans: Driving the sea surface temperature. *J. Phys. Oceanogr.,* **22,** 859–881.

Chang, P., L. Ji, and H. Li, 1997: A decadal climate variation in the Tropical Atlantic ocean from thermodynamic air–sea interactions. *Nature,* **385,** 516–518.

Chaves, R. R., and P. Nobre, 2004: Interactions between sea surface temperature over the South Atlantic Ocean and the South Atlantic Convergence Zone. *Geophys. Res. Lett.,* **31,** L03204, doi:10.1029/2003GL018647.

Corti, S., F. Molteni, and T. N. Palmer, 1999: Signature of recent climate change in frequencies of natural atmospheric circulation regimes. *Nature,* **398,** 789–802.

Da Silva, A. M., C. C. Young, and S. Levitus, 1994: *Algorithms and Procedures.* Vol. 1, *Atlas of Surface Marine Data,* NOAA Atlas NESDIS 6, 83 pp.

Diaz, A. F., C. D. Studzinski, and C. R. Mechoso, 1998: Relationships between precipitation anomalies in Uruguay and southern Brazil and sea surface temperature in the Pacific and Atlantic oceans. *J. Climate,* **11,** 251–271.

Drijfhout, S. S., A. Kattenberg, R. J. Haarsma, and F. M. Selten, 2001: The role of the ocean in midlatitude, interannual-to-decadal-timescale climate variability of a coupled model. *J. Climate,* **14,** 3617–3630.

Gandu, A. W., and P. L. Silva Dias, 1998: Impact of tropical heat sources on the South American tropospheric upper circulation and subsidence. *J. Geophys. Res.,* **103,** 6001–6015.

Gonçalves, F. L. T., P. L. Silva Dias, and G. P. Araújo, 2001: Climatological analysis of winter-time extreme low temperatures in São Paulo City, Brazil: Impact of SST anomalies. *Int. J. Climatol.,* **22,** 1511–1526.

Haarsma, R. J., and F. M. Selten, 2001: Mechanisms of extratropical decadal variability. *CLIVAR Exchanges*, No. 6, International CLIVAR Project Office, Southampton, United Kingdom, 8–11.

——, E. Campos, and F. Molteni, 2003: Atmospheric response to South Atlantic SST dipole. *Geophys. Res. Lett.,* **30,** 1864, doi:10.1029/2003GL017829.

Hastenrath, S., and L. Greischar, 1993a: Further work on the prediction of Brazilian rainfall anomalies. *J. Climate,* **6,** 734–758.

——, and ——, 1993b: Circulation mechanisms related to northeast Brazil rainfall anomalies. *J. Geophys. Res.,* **98,** 5093–5102.

Hoerling, M. P., J. W. Hurrell, and T. Xu, 2001: Tropical origins of recent North Atlantic climate change. *Science,* **292,** 90–92.

Houghton, J. T., Y. Ding, D. J. Griggs, M. Noguer, P. J. van der Linden, X. Dai, K. Maskell, and C. A. Johnson, Eds., 2001: *Climate Change 2001: The Scientific Basis.* Cambridge University Press, 881 pp.

Kalnay, E., and Coauthors, 1996: The NCEP/NCAR 40-Year Reanalysis Project. *Bull. Amer. Meteor. Soc.,* **77,** 437–471.

Latif, M., 2001: Tropical Pacific/Atlantic ocean interactions at multi-decadal time scales. *Geophys. Res. Lett.,* **28,** 539–542.

Lazar, A., R. Murtugudde, and A. Busalacchi, 2001: A model study of temperature anomaly propagation from the subtropics within the South Atlantic thermocline. *Geophys. Res. Lett.,* **28,** 1271–1274.

Levitus, S., and T. P. Boyer, 1994: *Temperature.* Vol. 4, *World Ocean Atlas 1994,* NOAA Atlas NESDIS 4, 117 pp.

——, R. Burgett, and T. P. Boyer, 1994: *Salinity.* Vol. 3, *World Ocean Atlas 1994,* NOAA Atlas NESDIS 3, 99 pp.

Mo, K. C., and S. Häkkinen, 2001: Decadal variations in the tropical South Atlantic and linkages to the South Pacific. *Geophys. Res. Lett.,* **28,** 2065–2068.

Molteni, F., 2003: Atmospheric simulations using a GCM with simplified physical parametrizations. I: Model climatology and variability in multi-decadal experiments. *Climate Dyn.,* **20,** 175–191.

Moron, V., R. Vautard, and M. Ghil, 1998: Trends, interdecadal and interannual oscillations in global sea-surface temperatures. *Climate Dyn.,* **14,** 545–569.

Moura, A. D., and J. Shukla, 1981: On the dynamics of droughts in northeast Brazil: Observations, theory and numerical experiments with a general circulation model. *J. Atmos. Sci.,* **38,** 2653–2675.

Niiler, P. P., and E. B. Kraus, 1977: One-dimensional models of the upper ocean. *Modeling and Prediction of the Upper Layers of the Ocean,* E. B. Kraus, Ed., Pergamon, 143–172.

Nobre, P., and J. Shukla, 1996: Variations of sea surface temperature, wind stress, and rainfall over the tropical Atlantic and South America. *J. Climate,* **9,** 2464–2479.

Okumura, Y., S.-P. Xie, A. Numaguti, and Y. Tanimoto, 2001: Tropical Atlantic air–sea interaction and its influence on the NAO. *Geophys. Res. Lett.,* **28,** 1507–1510.

Palastanga, V., C. S. Vera, and A. Piola, 2002: On the leading modes of sea surface temperature variability in the South Atlantic ocean. *CLIVAR Exchanges*, No. 7, International CLIVAR Project Office, Southampton, United Kingdom, 12–15.

Rajagolapan, B., Y. Kushnir, and Y. M. Tourre, 1998: Observed decadal midlatitude and Tropical Atlantic climate variability. *Geophys. Res. Lett.,* **25,** 3967–3970.

Robertson, A. W., and C. R. Mechoso, 1998: Interannual and decadal cycles in river flows of southeastern South America. *J. Climate,* **11,** 2570–2581.

——, and ——, 2000: Interannual and interdecadal variability of the South Atlantic convergence zone. *Mon. Wea. Rev.,* **128,** 2947–2957.

——, ——, and Y.-J. Kim, 2000: The influence of Atlantic sea surface temperature anomalies on the North Atlantic oscillation. *J. Climate,* **13,** 122–138.

——, J. D. Farrara, and C. R. Mechoso, 2003: Simulations of the atmospheric response to South Atlantic sea surface temperature anomalies. *J. Climate,* **16,** 2540–2551.

Ruiz-Barradas, A., J. A. Carton, and S. Nigam, 2000: Structure of interannual-to-decadal climate variability in the tropical Atlantic sector. *J. Climate,* **13,** 3285–3297.

Seager, R., M. B. Blumenthal, and Y. Kushnir, 1995: An advective atmospheric mixed layer model for ocean modeling purposes: Global simulation of surface heat fluxes. *J. Climate,* **8,** 1951–1964.

Sterl, A., 2001: Decadal variability in the South Atlantic ocean. *CLIVAR Exchanges*, No. 6, International CLIVAR Project Office, Southampton, United Kingdom, 20–22.

——, and W. Hazeleger, 2003: Coupled variability and air–sea interaction in the South Atlantic ocean. *Climate Dyn.,* **21,** 559–571.

Tourre, Y. M., B. Rajagopalan, and Y. Kushnir, 1999: Dominant patterns of climate variability in the Atlantic Ocean during the last 136 years. *J. Climate,* **12,** 2285–2299.

Venegas, S. A., L. A. Mysak, and D. N. Straub, 1996: Evidence for interannual and interdecadal climate variability in the South Atlantic. *Geophys. Res. Lett.,* **23,** 2673–2676.

——, ——, and ——, 1997: Atmosphere–ocean coupled variability in the South Atlantic. *J. Climate,* **10,** 2904–2920.

——, ——, and ——, 1998: An interdecadal climate cycle in the South Atlantic and its links to other basins. *J. Geophys. Res.,* **103,** 24 723–24 736.

Wainer, I., and S. Venegas, 2002: South Atlantic variability in the climate system model. *J. Climate,* **15,** 1408–1420.

Wang, J., and J. A. Carton, 2003: Modeling climate variability in the tropical Atlantic atmosphere. *J. Climate,* **16,** 3858–3876.

Watanabe, M., and M. Kimoto, 1999: Tropical–extratropical connection in the Atlantic atmosphere–ocean variability. *Geophys. Res. Lett.,* **26,** 2247–2250.

Xie, S.-P., 1999: A dynamic ocean–atmosphere model of the tropical Atlantic decadal variability. *J. Climate,* **12,** 64–70.

——, and Y. Tanimoto, 1998: A pan-Atlantic decadal climate oscillation. *Geophys. Res. Lett.,* **25,** 2185–2188.